J Braz. Soc. Mech. Sci. Eng. (2014) 36:13–22
DOI 10.1007/s40430-013-0061-7

TECHNICAL PAPER

The influence of geometrical and operational parameters on Y-jet atomizers performance

Antonio L. Pacifico · Jurandir I. Yanagihara

Received: 19 April 2013 / Accepted: 20 July 2013 / Published online: 7 August 2013

Abstract The effects of operational and geometrical parameters on pressure distribution and flow pattern in Y-jet atomizers were studied using an experimental apparatus working with air and water. The results show that the mixing point pressure is very dependent on the diameter ratio of the mixing duct and the air port and the water supply pressure ratio. A correlation to predict the mixing point pressure was developed and showed good agreement with the experimental data. With this correlation, it is possible to predict the occurrence of the critical condition for the air flow at the exit of its port. In a second group of results, the influence of geometrical and operational parameters on the pressure distribution inside the mixing duct was analyzed. The main result found was that for air liquid ratio between 0.1 and 0.2, this pressure distribution can be taken as linear. This information about air liquid ratio and the correlation to predict the occurrence of chocked flow at the exit of the air port may give useful guidelines for atomizer designers. Finally, using a two-phase map, the flow pattern inside Y-jet atomizers was found to be a transition between the annular flow and the wispy-annular flow.

Keywords Y-jet atomizers · Twin-fluid atomizers · Two-phase flow patterns · Experimental correlations

Technical Editor: Luis Fernando Figueira da Silva.

A. L. Pacifico · J. I. Yanagihara (✉)
Department of Mechanical Engineering, Polytechnic School, University of São Paulo, Av. Prof. Mello Moraes, 2231, São Paulo 05508-970, Brazil
e-mail: jiy@usp.br

List of symbols

ALR	Air liquid ratio
d	Diameter [m]
G	Fluid mass velocity [kg/m^2 s]
j	Superficial velocity [m/s]
l	Length [m]
p	Pressure [Pa]
SR	Slope ratio
T	Temperature [K]
$\dot{m}$	Mass flow rate [kg/s]
z	Position [m]

Non-dimensional groups

We	Weber number

Greek symbols

γ	Ratio of specific heats
Δp	Pressure drop [Pa]
θ	Angle between air and water ports [rad]
ρ	Density [kg/m^3]
φ	Momentum ratio

Subscripts

1	Middle point pressure measurement in mixing duct
2	End point pressure measurement in mixing duct
a	Air
w	Water
ha	Air at upstream position of the tape orifice plate
M	Mixing point
m	Mixing duct

1 Introduction

There are basically two types of atomizers that are widely used to burn heavy fuel oils: mixing chamber and Y-Jet atomizers. Y-jet atomizer is a twin fluid atomizer, largely

used in industrial burners which consume medium heavy and light fuel oils, and operates with air or steam as auxiliary fluid. Y-Jet atomizers are known for their ability to maintain moderate emission rates while attaining a relatively high efficiency in the atomization process. The low atomizing fluid consumption is also a positive feature of Y-Jet atomizers. This is possible in Y-Jet atomizers because of the closer contact between atomizing fluid and auxiliary fluid and low auxiliary fluid consumption [1, 2, 13]. The key factor here is the momentum transfer inside the nozzle: the more efficient this momentum transfer is from the auxiliary fluid to the fuel, the better the spray quality will be regarding spatial drops distribution and the mean drop size diameter.

Andreussi et al. [1], Mullinger and Chigier [14] and Song and Lee [16] showed that the momentum transfer efficiency is determined mainly by (1) the air to liquid ratio, ALR; (2) the angle θ between the ports of fuel and auxiliary fluid; (3) the ratios between the geometric parameters of the Y-Jet atomizer such as length to diameter of the mixing duct l_m/d_m, mixing duct to auxiliary fluid port diameters d_m/d_a, and so on.

Mullinger and Chigier [14] and Andreussi et al. [1] determined how the symmetry and the liquid film thickness inside the mixing duct influence spray characteristics externally to the nozzle, showing a close connection between both flows. Song and Lee [16] made a photographic study of the flow patterns inside and outside the Y-jet atomizers and were able to determine the main mechanisms involved in the fuel atomization.

Song and Zhang [17] worked on a one-dimensional, separated-phase model for the flow inside Y-Jets and combined it with a uniform atomization model outside the nozzle by introducing an analysis of the growth rate of the surface disturbance.

Recently, Zhou et al. [19] have worked on an experimental investigation of the atomization performance of single-hole Y-Jet nozzle. Although they have found interesting results for the dependence of the droplet mean diameter of the sprays on the air–liquid ratio, they did not take into account the mechanisms of the internal flow that could influence the spray quality.

In order to study and to design Y-jet atomizers, it is important to know the flow behavior inside the mixing duct. Particularly, the information about the flow pressure at the mixing point and along the mixing duct, thus characterizing the pressure drop, is very important to yield hypotheses that are simple and accurate. By using an especially constructed experimental apparatus, this research aimed to study how some geometrical parameters, such as the diameter ratio of the mixing duct and the air port and the angle between the water port and the mixing duct, influence the flow pattern and pressure distribution in the mixing duct of Y-jet atomizers.

2 Experimental apparatus and setup

In a schematic drawing, Fig. 1 shows the experimental apparatus used in the present experiment. Air and water

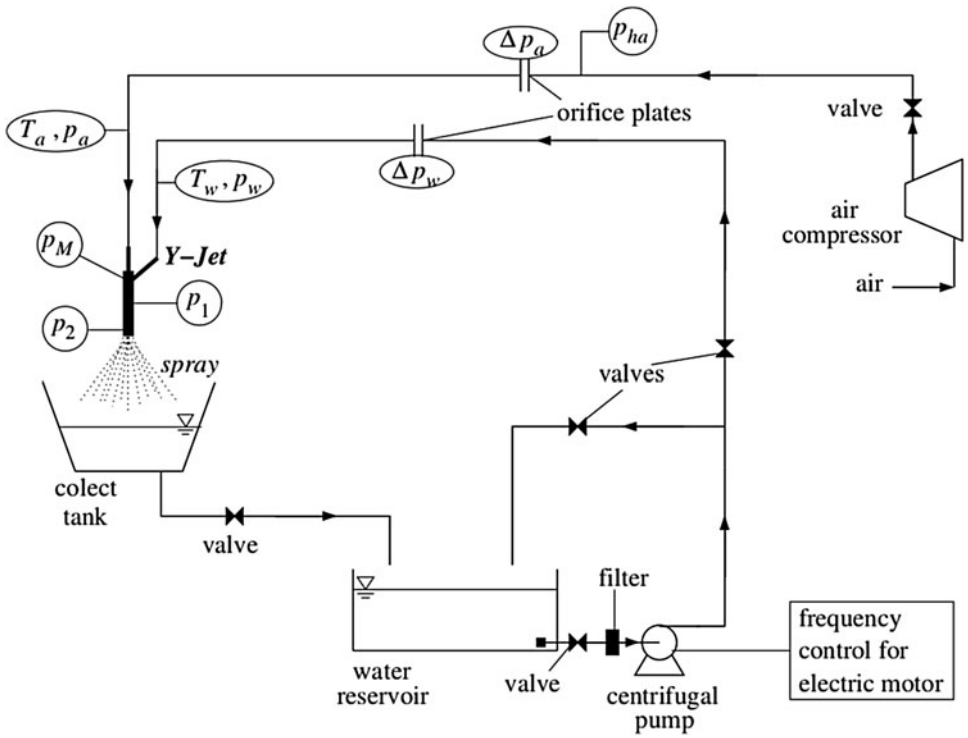

Fig. 1 Schematic drawing of the experimental apparatus used in the tests

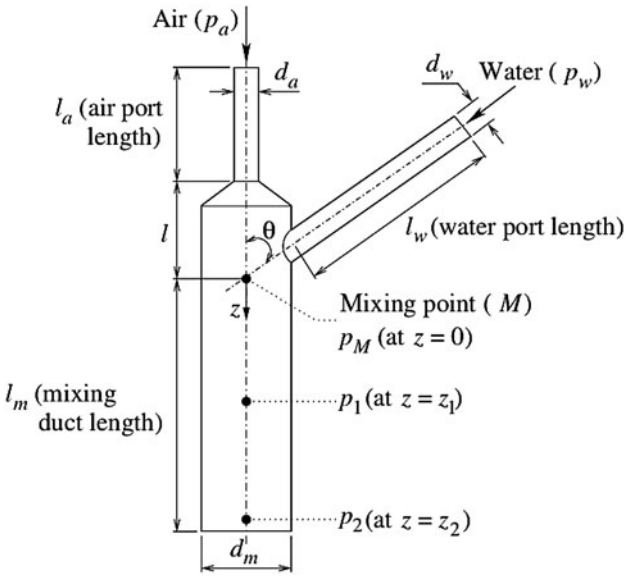

Fig. 2 Schematic drawing of the generic Y-jet atomizer used in this work

were the working fluids. Air and water mass flow rates (W_a and W_w, respectively) were measured by corner tap orifice plates according to BS 1042, Sections 1.1 and 1.2 [3]. Through the frequency control of the pump driving electric motor and by adjusting the two valves upstream the pump, it was possible to obtain the desired levels of water mass flow rate and its pressure supply (p_w). The air mass flow rate was obtained from its pressure supply (p_a)—there was an electronic adjustment in the compressor—and the pressure drop of the air line. In the same figure, T_a and T_w represent the air and water supply temperatures, respectively. All the experiments were conducted at room temperature. The ranges of pressures used were from 4.7 to 11.7 bar for p_a and from 1.5 to 17 bar for p_w. The spray was discharged in the laboratory environment, i.e., at atmospheric pressure.

In order to allow parametric analysis, seven Y-jet atomizers were constructed according to design criteria from Mullinger and Chigier [14]. A schematic drawing of the tested nozzles can be seen in Fig. 2. Table 1 shows the main values of the geometrical parameters used. All the pressure points, i.e., p_a, p_w, p_M, p_1 and p_2, were measured by piezo-resistive transducers, where p_M is the mixing point pressure, p_1 the pressure at the middle point in the mixing duct and p_2 the pressure near the end of the mixing duct. The pressure transducers (Danfoss AKL-33 060-g2105 and AKL-33 060-g2104) had a full-scale precision of 0.3 %. The transducers were connected to the nozzles' pressure taps (diameter = 1 mm) by flexible tubes. Table 1 shows their exact positions in the mixing duct (z_1 for p_1 and z_2 for p_2).

The atomizers were manufactured using a 3:1 scale in order to allow easier access to the pressure and temperature sensors, without perturbing the flow. To maintain a comparison basis with geometrical and operational parameters used in the literature [1, 14, 16] a non-dimensional analysis based on the Weber number, *We*, for the air flow inside the mixing duct was conducted. According to the above cited works, the minimum and maximum values for *We* were on the order of magnitude of 10^2 and 10^4, respectively. In this work, the range for *We* was 500–42,500. Also, the air and water fluid mass velocities, G_a and G_w respectively, were imposed in the same order of magnitude to those used in the literature, that is 10^2–10^3 for G_a and 10^2–10^4 for G_w. Thereby, the following mass flow rates ranges were applied in order to obtain these criteria: $40 < \dot{m}_a < 320\,\mathrm{kg/h}$ and $240 < \dot{m}_w < 2,600\,\mathrm{kg/h}$.

For the seven nozzles, the main geometrical parameters studied were as follows: the water port to the mixing duct entry angle (θ); the ratio between the mixing duct length and diameter (l_m/d_m); and the ratio between the mixing duct and the air port diameters (d_m/d_a) that include the effects of the air flow expansion from the air port to the mixing duct. The ranges used for the tests of these geometric parameters were $\pi/4 \le \theta \le 7\pi/18$ (45°–70°); $3.5 \le l_m/d_m \le 10$; and $1.67 \le d_m/d_a \le 2$. The following sets of atomizers were used for each parametric study: nozzles 2, 4 and 5 for θ; nozzles 2, 6 and 7 for l_m/d_m; and nozzles 1, 2 and 3 for d_m/d_a. These values are shown in Table 1 for each nozzle.

Table 1 Geometrical values for the parameters in Fig. 2

Y-jet Atomizer	l_c (mm)	l (mm)	l_m (mm)	d_a (mm)	d_m (mm)	θ	l_m/d_m	d_m/d_a	z_1 (mm)	z_2 (mm)
1	40	13.5	50	5.5	10	57°	5.00	1.82	25	42.5
2	50	14.0	50	6.0	10	57°	5.00	1.67	25	42.5
3	50	14.7	50	6.0	12	57°	4.17	2.00	25	42.5
4	50	16.7	50	6.0	10	45°	5.00	1.67	25	42.5
5	50	12.1	50	6.0	10	70°	5.00	1.67	25	42.5
6	50	14.1	35	6.0	10	57°	3.50	1.67	–	27.5
7	50	14.0	100	6.0	10	57°	10.00	1.67	50	92.5

Table 2 Standard uncertainties for the measured variables

Variable	p_a (bar)	T_a (°C)	p_w (bar)	T_w (°C)	p_M (bar)	p_1 (bar)	p_2 (bar)	Δp_a (mbar)	Δp_w (mbar)	p_{ha} (bar)
Expanded Uncertainty	0.018	0.31	0.30	0.32	0.019	0.018	0.013	0.070	0.075	0.018

Table 2 shows the standard uncertainties of the measured variables. These uncertainties were calculated according to the JCGM [11].

3 Results and discussion

The results for the p_M/p_a and p_w/p_a ratios as function of the air liquid ratio, ALR ($= \dot{m}_a/\dot{m}_w$), are shown in Figs. 3 and 4, respectively.

In qualitative terms, all the results are similar, i.e., p_M and p_w decrease with the increment of ALR. This behavior occurs because the increment of ALR is the result of the increment of $\dot{m}_a$ or the decrement of $\dot{m}_w$, which induces the air flow momentum to have a larger influence on the mixing process, and particularly on the mixing point pressure. On the other hand, as the water flow determines the back pressure for the air expansion, the value of the ratio p_w/p_a is also important. This behavior is intrinsic to any compressible fluid expansion and leads to the conclusion that p_M is controlled, among others, by the water flow rate in the mixing point.

In Fig. 3, it can also be seen that there are values for p_M/p_a smaller than 0.5283 (for ALR > 0.25), in all the cases studied. The hypothesis here is that the flow from the air port to the mixing point is single phase (air only) with $\gamma = 1.4$, where γ is the ratio of specific heats. This critical condition happens because of the air port geometry and the air flow discharge in the mixing duct. These nozzles in Y-jet atomizer are similar to a converging–diverging nozzle, where the air port (d_a) acts as a nozzle throat and the mixing point pressure (p_M) as the back pressure in the diverging passage (controlled by the water flow in this region).

There is virtually no difference among the results of the influence of θ on p_M/p_a as a function of ALR, concluding that θ does not exert significant influence on the mixing point pressure. Regarding the influence of l_m/d_m on p_M/p_a as a function of ALR, the results indicate that p_M increases with the rise of l_m/d_m since the pressure drop inside the mixing duct is smoother for larger values of l_m. Thus, the environmental pressure being the same for the nozzles (i.e., the atmospheric pressure), the atomizers with higher l_m also have higher values for p_M. Finally, it has been confirmed that the influence of d_m/d_a on p_M is the most significant of all the geometrical relations studied here. Higher values of d_m/d_a produce higher values of the pressure drop between the air pressure supply (p_a) and the pressure in the mixing point (p_M). Particularly, in the range $0.1 < \text{ALR} < 0.4$, the influence of d_m/d_a is more

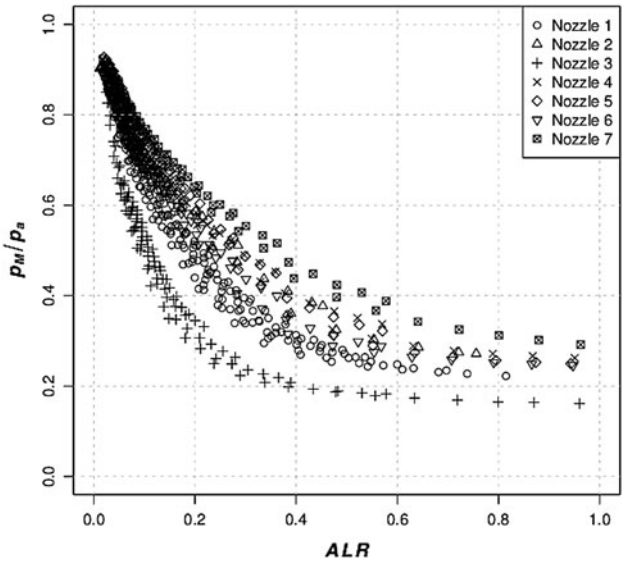

Fig. 3 Experimental results for p_M/p_a as a function of ALR for all the tested nozzles

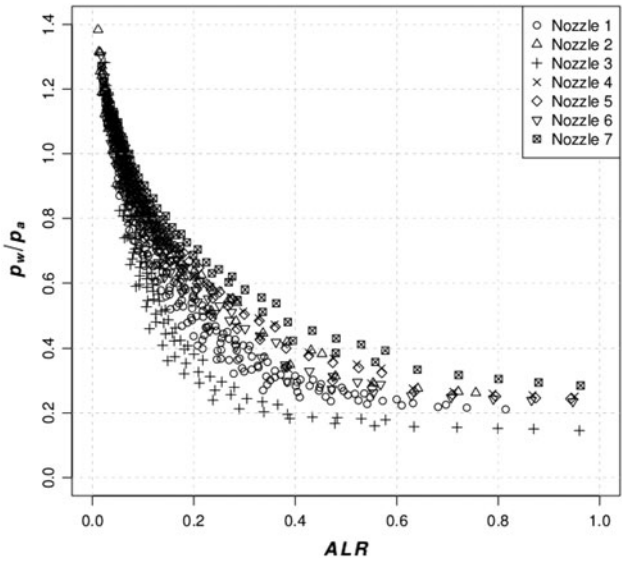

Fig. 4 Experimental results for p_w/p_a as a function of ALR for all the tested nozzles

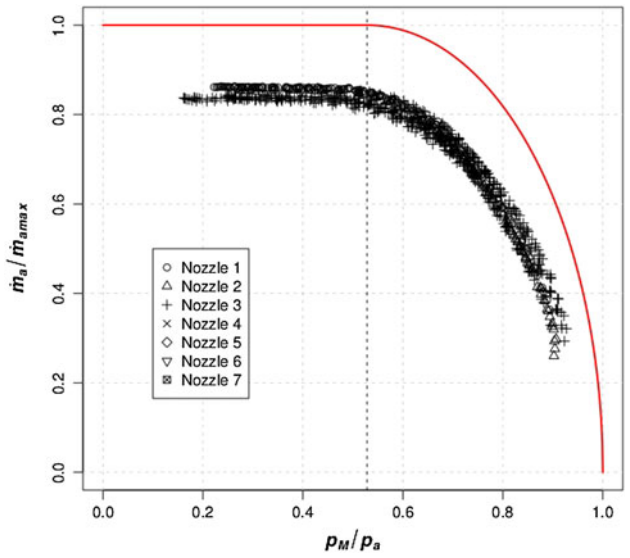

Fig. 5 Actual and maximum air mass flow ratio as a function of the pressure ratio in the expansion from air duct to the mixing duct

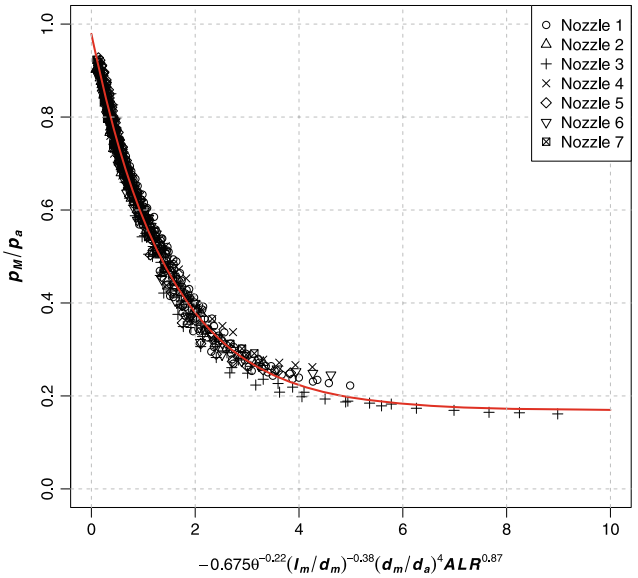

Fig. 6 Comparison between results using Eq. (1) and experimental results

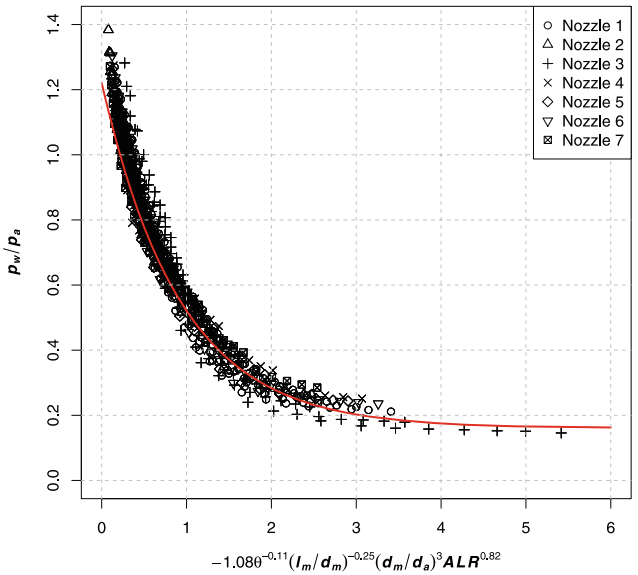

Fig. 7 Comparison between results using Eq. (2) and experimental results

remarkable, indicating that the air pressure drop in this region is larger when d_m/d_a is incremented. Similarly, the p_w/p_a as a function of ALR has the same behavior of that found for p_M/p_a for the geometrical parameters analyzed (Fig. 4).

Figure 5 shows the ratio of air mass flow rate (actual $\dot{m}_a$) to the maximum air mass flow rate (for Mach number equal to one at the throat—air port, $\dot{m}_{amax}$) as a function of pressure ratio p_M/p_a. In the same figure, in continuous line, the curve for isentropic compressible flow is also plotted. In order to show the data inside the shocked region, a dashed line was drawn for $p_M/p_a = 0.5283$. The deviation of the data from the isentropic prediction line is due to the sudden expansion of air from its port to the mixing duct.

It is also to be considered if the presence of water inside the duct could restrict the air flow. Ferreira et al. [5, 6] showed that the liquid mass flow rate changes the value of the gas mass flow rate at which the flow is choked, for the same geometric expansion relation (d_m/d_a). However, the chocked condition always occurs at the exit of air port, not downstream this point. In fact, the mixing point pressure is established by three key factors: liquid (water) and gas (air) mass flow rates and d_m/d_a relation. The same authors comment that the smallest values for Sauter Mean Diameters in the spray are observed when the nozzles operate at chocked conditions, meaning that this is an important parameter for the operation of these nozzles.

In order to show the influence of all the parameters analyzed in Figs. 3 and 4 in a single curve, two correlations for the p_M/p_a and p_w/p_a were proposed. Figures 6 and 7 show these correlations for p_M/p_a and p_w/p_a, respectively, along with the results obtained for nozzles 1–7. These correlations are

$$\frac{p_M}{p_a} = 0.169 + 0.81\exp\left[-0.675\theta^{-0.22}\left(\frac{l_m}{d_m}\right)^{-0.38}\left(\frac{d_m}{d_a}\right)^4 \mathrm{ALR}^{0.87}\right] \quad (1)$$

$$\frac{p_w}{p_a} = 0.161 + 1.06\exp\left[-1.08\theta^{-0.11}\left(\frac{l_m}{d_m}\right)^{-0.25}\left(\frac{d_m}{d_a}\right)^3 \mathrm{ALR}^{0.82}\right]. \quad (2)$$

The correlations shown in Eqs. (1) and (2) are valid for the following range: $0 \leq \mathrm{ALR} \leq 1$; $3.5 \leq l_m/d_m \leq 10$; $1.67 \leq d_m/d_a \leq 2$; and $45^o < \theta < 70^o$. In the correlations, θ must be given in radians ($\pi/4 < \theta < 7\pi/18$). As can be seen in Figs. 6 and 7, there is good agreement between the experimental points and the correlations given by Eqs. (1) and (2).

An important design parameter is the condition for critical air flow. For the present case, $p_M/p_a < 0.5283$ (critical condition) is obtained when $\theta^{-0.22}(l_m/d_m)^{-0.38}\,(d_m/d_a)^4\mathrm{ALR}^{0.87} > 1.2$.

The same behavior found for p_M/p_a against ALR was found for p_1/p_a and p_2/p_a against ALR, suggesting a more general correlation grouping, beyond the parameters used in Eqs. (1) and (2), also the z coordinate (Fig. 2), thus resulting in a correlation that allows predicting the pressure evolution within the whole mixing duct. This general correlation is shown in Eq. (3)

$$\frac{p(z)}{p_a} = 0.172 + 0.732\exp\left[-0.371\theta^{-0.203}\left(\frac{l_m}{d_m}\right)^{-0.422} \times \left(\frac{d_m}{d_a}\right)^{5.152}\mathrm{ALR}^{0.988} - 1.286\left(\frac{z}{l_m}\right)^{1.251}\right]. \quad (3)$$

There is another operational parameter commonly accepted for Y-Jet atomizers: the ratio between the lateral momentum of the liquid jet going inside the mixing duct and the axial momentum of the auxiliary fluid (air or steam), known in the literature by the symbol φ. Mathematically,

$$\varphi = \frac{G_w^2 d_w^2 \rho_{a,M}\sin\theta}{G_{a,M}^2 d_m^2 \rho_w} \quad (4)$$

where G_w is the liquid (water) mass velocity, d_w is the liquid port diameter, ρ_w is the liquid density, $G_{a,m}$ is the gas (air) mass velocity, d_m is the mixing duct diameter and $\rho_{a,m}$ is the gas density evaluated at the average pressure between p_M and p_{atm} and at mixing temperature, T_M, calculated by,

$$T_M = \frac{\dot{m}_a C_{p,a} T_a + \dot{m}_w C_{p,w} T_w}{\dot{m}_a C_{p,a} + \dot{m}_w C_{p,w}} \quad (5)$$

where $C_{p,a}$ and $C_{p,w}$ are the specific heats of gas and liquid, respectively.

This ratio was introduced by Graziadio et al. [7] and Andreussi et al. [1] and, according to these authors, this parameter exerts a strong influence on the quality and structure of the spray outside the atomizer. Thus, another general correlation was developed replacing ALR by φ. The result was

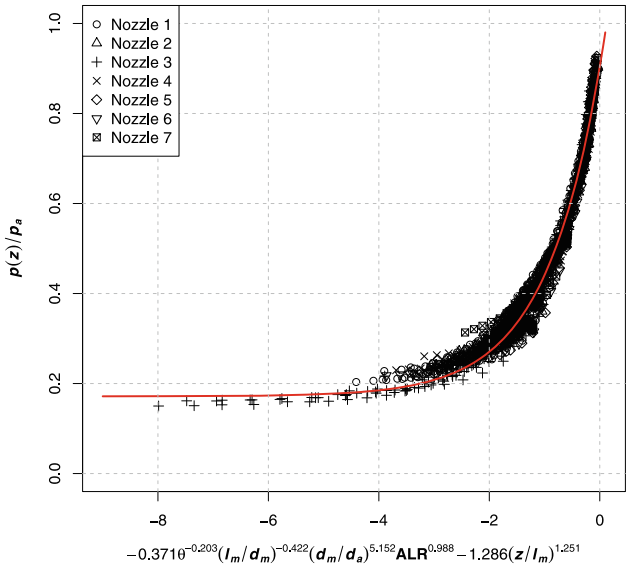

Fig. 8 Comparison between results using Eq. (3) and experimental results

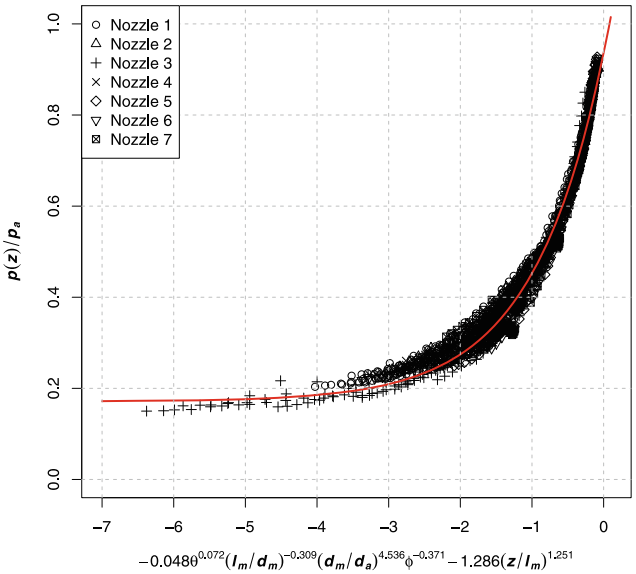

Fig. 9 Comparison between results using Eq. (6) and experimental results

$$\frac{p(z)}{p_a} = 0.172 + 0.764\exp\left[-0.048\theta^{0.072}\left(\frac{l_m}{d_m}\right)^{-0.309} \times \left(\frac{d_m}{d_a}\right)^{4.536}\varphi^{-0.371} - 1.286\left(\frac{z}{l_m}\right)^{1.251}\right] \quad (6)$$

Comparing Eqs. (3) and (6), the first terms and those related with the z/l_m parameter are identical meaning that the use of ALR or φ only changes how the l_m/d_m and d_m/d_a influence the pressure distribution inside the mixing duct.

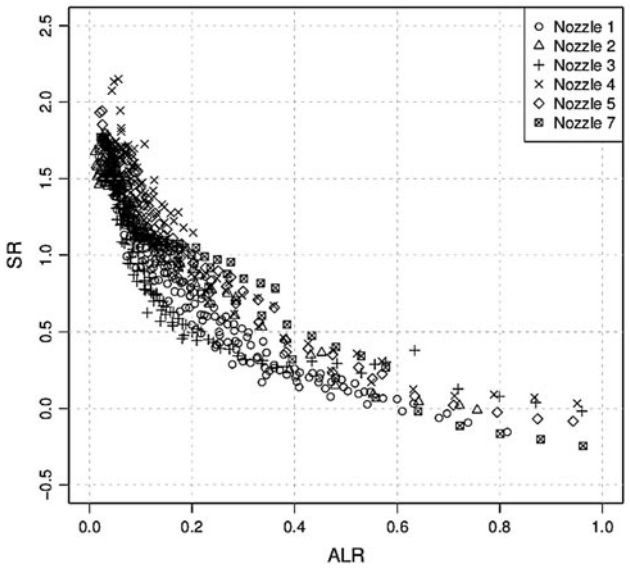

Fig. 10 Slope ratio, *SR*, as a function of ALR

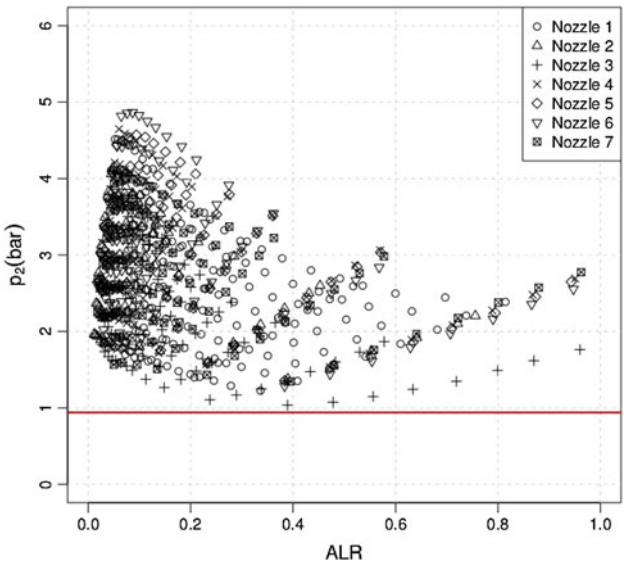

Fig. 11 Comparison between results for p_2 and the atmospheric pressure level (*line*) for all the nozzles (color figure online)

Figures 8 and 9 show the results of the experimental values (dots) for all the nozzles and the predicted values (line) by Eqs (3) and (6). The agreement between those results is very good. The residual standard errors found were 0.02226 for Eq. (3) and 0.02236 for Eq. (6).

Another interesting result is that the pressure distribution inside the mixing duct can be taken as linear if $0.1 < \text{ALR} < 0.2$. This behavior can be observed in Fig. 10 that shows the slope ratio (SR) of the pressure evolution within the mixing duct as a function of ALR. This slope ratio is given by the following relationship

$$\text{SR} = \frac{(p_\text{M} - p_1)(z_2 - z_1)}{(p_1 - p_2)(z_1 - z_\text{M})} \tag{7}$$

where z_M, z_1 and z_2 are, respectively, the locations of the tap for mixing point pressure, p_M, middle point pressure, p_1, and near end pressure of the mixing duct, p_2—see Fig. 2 and Table 1.

The SR is an important parameter for this kind of analysis because it can indicate the regions where the pressure distribution is approximately linear. In the present results, this region is in the range of $0.1 < \text{ALR} < 0.2$. Because the range $0.05 < \text{ALR} < 0.3$ is the most used in practice (most widely used works with 0.08), this provides an important direction for the mathematical modeling of pressure drop inside the mixing duct of Y-jet atomizers. It should be taken into account that nozzle 6 is not part of this analysis for not having the middle point pressure, p_1 (see Table 1).

Finally, to close the analysis of the pressure distribution inside the mixing duct, Fig. 11 shows the values of p_2 for all the nozzles tested comparing them with the atmospheric pressure (in red). The mean atmospheric pressure at the site of the experiments was 94.4 kPa with insignificant standard deviation (<0.34 %). The results indicate high pressure levels of p_2 in the exit region of the atomizer, for the small values of ALR. For these cases, a kind of accommodation must occur at the end of the mixing duct for the pressure to reach the atmospheric value. As the flow at this region is a two-phase flow, the hypothesis of chocked flow—normal and oblique chock waves—must be rejected, as it has been observed only for solid particles and gas mixtures, as those involved in solid propellants [18]. Also the critical phenomena in two-phase flows are less well defined—e.g. pressure propagation—as proposed by Hewitt and Hall-Taylor [10].

The combined uncertainties for the parameters presented in this section are summarized in Table 3. Their values are dependent on the levels of the mass flow rates. Thus, as example, they are shown for two values of φ.

In order to further explore the flow within the mixing duct, some appropriate two-phase flow maps were analyzed. Figures 12, 13 and 14 show vertical two-phase flow pattern maps for water and air extracted from [9], Fig. 12; [8], Fig. 13; and [15], Fig. 14.

In Fig. 12, the coordinates present the superficial momentum fluxes for the air (ordinate) and water (abscise). j_a and j_w are the superficial velocities for air and water, respectively. The specific mass of the air, ρ_a, was calculated as the average value between the mixing point (at mixing point pressure, p_M) and the exit of the mixing duct (at atmospheric pressure, p_atm). Although the tests were carried out in a vertical downward orientation, the influence of the gravity compared to the momentum transfer was found to be minimal inside the mixing duct. The

Table 3 Examples of combined uncertainties for the parameters

Parameter	$\varphi \sim 3$		$\varphi \sim 11$	
	Value	Combined uncertainty	Value	Combined uncertainty
$\dot{m}_a$ (kg/h)	106.1	0.3	82.8	0.4
$\dot{m}_w$ (kg/h)	2,001.5	4.4	2,679.0	4.2
ALR	0.053	0.0002	0.031	0.0002
p_M/p_a	0.648	0.008	0.808	0.008
φ	3.03	0.09	11.05	0.33

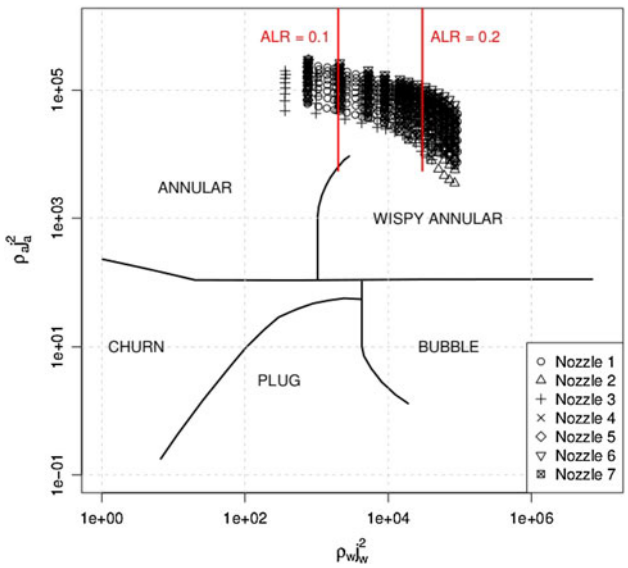

Fig. 12 Vertical two-phase flow pattern according [9]

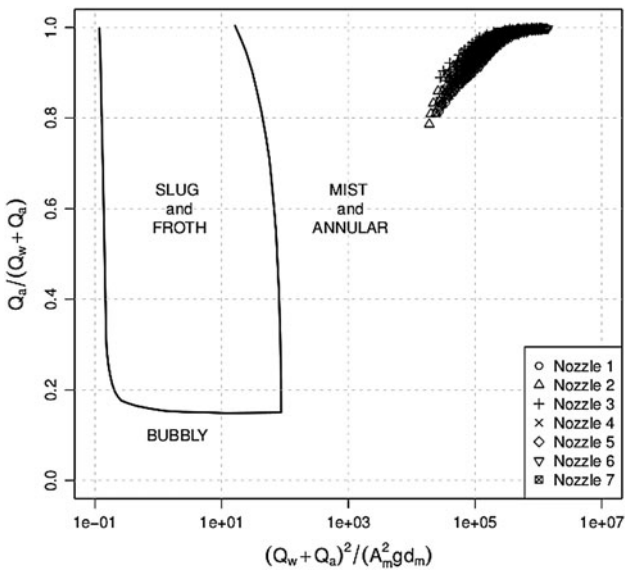

Fig. 13 Vertical two-phase flow pattern according [8]

results shown in this figure stand for all the seven nozzles tested. It can be seen that the main flow patterns are the annular and the wispy-annular. In terms of $\rho_w \cdot j_w^2$, ALR

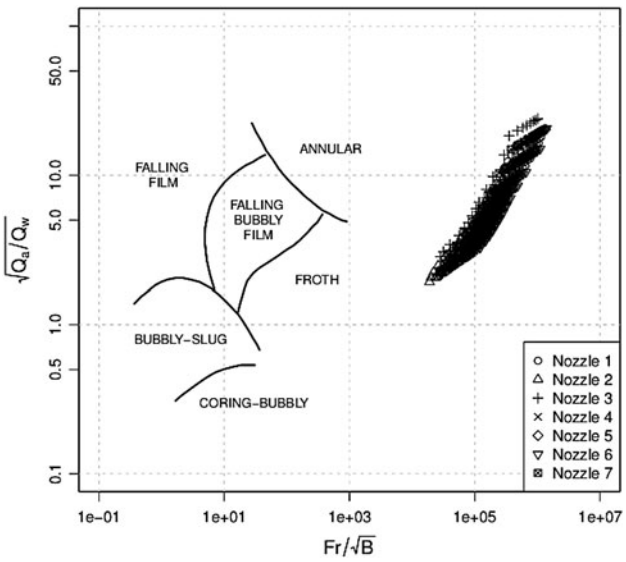

Fig. 14 Vertical two-phase flow pattern according [15]

increases with the decrement of $\rho_w \cdot j_w^2$. Then, according to this map, for small values of ALR, the main flow pattern is a transition between the annular flow and the wispy-annular flow. The region of interest, that is $0.1 < \text{ALR} < 0.2$ for practical applications, occurs exactly above this transition. It should be noted that these boundaries in the two-phase maps are not exact [4].

Figure 13 shows the results for the Griffith and Wallis [8] map. In this figure, Q_a and Q_w are the volumetric flow rates of air and water, respectively; d_m and A_m are the diameter and cross-sectional area of the mixing duct, respectively; and g the acceleration of gravity. According to the flow patterns described by this map, the results are localized in the mist and annular regions, for high values of $Q_a/(Q_a + Q_w)$, meaning that Q_a and $Q_a + Q_w$ have the same order of magnitude. This condition, in which the volume occupied by the air fraction is larger than that occupied by the water, constitutes a typical atomizer flow pattern.

For the results shown in Fig. 14, Q_a and Q_w are the volumetric flow rates of air and water, respectively; Fr is the Froud number and B, given by

$$B = \frac{\mu_{\text{liquid}}/\mu_{\text{water}}}{\left[(\rho_{\text{liquid}}/\rho_{\text{water}})(\sigma_{\text{liquid-air}}/\sigma_{\text{water-air}})^3\right]^{1/4}} \quad (8)$$

where μ is the absolute viscosity; and σ is the surface tension. As in this work, the liquid used was water, $B = 1$. In this map, only Fr is taken into account in the abscissa, therefore meaning that only the influence of the gravitational field on the flow is considered.

The results are outside the flow regimes established by the map although it is possible to say that they are in the region of transition between froth and annular. This transition occurs for the values of mass flow rate of water greater than 1,000 kg/h and for ARL smaller than 0.1. As the water mass flow rate decreases, ALR increases and it is reasonable to speculate that the flow leaves the annular zone to become dispersed. According to Oshinowo and Charles [15], for $\dot{m}_w > 1,000\,\text{kg/h}$ (or $\text{ALR} < 0.1$) the flow pattern would be a mixture of froth and annular (maybe the "wispy annular"), for $500 < \dot{m}_w < 1,000\,\text{kg/h}$ $(0.1 < \text{ALR} < 0.3)$, the flow pattern would be a more defined annular and for $\dot{m}_w < 500\,\text{kg/h}$ (or $\text{ALR} > 0.3$), the flow would be found in the atomized region. Obviously, these conclusions are merely speculative, once the results were founded outside the map.

All the maps suggest a pattern near the atomized region. Although these maps were not plotted specifically for flows inside Y-jet atomizers, they can yield important information to improve the existing models and their results. Concerning the unsteady sprays caused by transitions between two-phase flow patterns, two-phase flows become unsteady when inhomogeneity is present in the mixture of phases. Jedelsky and Jicha [12] presented a detailed analysis regarding spray unsteadiness for effervescent atomizers. Although effervescent atomizers operate at lower pressures as compared to Y-jet atomizers, some important findings of their work can be brought in order to elucidate this problem. One important conclusion in the context of the present work is that the unsteadiness grows as ALR decreases, which is also accompanied by the increase in the liquid discharge coefficient. They found spray unsteadiness for $\text{ALR} < 0.06$. Another important remark is that the increase of fluctuations of void fraction at the exit port of the nozzle produces unsteadiness on the spray. This phenomenon also occurs for very small or very large values of ALR. At these extremes, large structures of separated phases are present, constituting inhomogeneous mixture, which in turn causes great variations in the volume of the compressed air and formation of large clusters of liquid (ligaments) at the exit of the nozzle. Therefore, it is important to operate Y-jet atomizers far from these extremes of ALR. A practical consequence from the point of view of the results shown in Fig. 12 would be to operate Y-jet atomizers for $0.1 < \text{ALR} < 0.2$. In this range, the two-phase flow pattern will be annular mist (Fig. 13), far from annular to wispy-annular transition, avoiding the appearance of large ligaments of liquid and constituting more homogeneous and steady sprays.

4 Conclusions

In this study, the influence of the operational and geometric parameters on the pressure distribution and flow pattern inside the mixing duct of Y-jet atomizers was carefully examined. Air and water were the working fluids. Water supply pressure exerts great influence on the mixing point pressure, acting as a back pressure for the air expansion, if one considers a converging–diverging nozzle analogy. The ratio between the mixing duct and the air port diameters was the main geometric parameter that regulated the mixing duct pressure. The correlation developed to foresee the mixing point pressure [Eq. (1)] as a function of operational and geometric parameters studied, showed to agree well with the experimental results.

An important design parameter is the condition for critical air flow. For the present case, $P_M/P_a < 0.5283$ (critical condition) is obtained when $\theta^{-0.22}(l_m/d_m)^{-0.38}(d_m/d_a)^4\text{ALR}^{0.87} > 1.2$.

Two correlations for the prediction of the pressure within the mixing duct were developed and showed good agreement with the experimental values. This is important because they can be used to model the pressure drop in this region, thus helping in the design of Y-jet atomizers.

For $0.1 < \text{ALR} < 0.2$, the pressure distribution inside the mixing duct can be taken as linear. This range of ALR is the most appropriate to obtain steady and homogeneous flows. For $\text{ALR} < 0.1$, this pressure drop is larger in the first half of the mixing duct, being the opposite for $\text{ALR} > 0.2$.

The high pressure levels for the pressure near the end of the mixing duct suggests that a kind of relaxation must occur in order to accommodate the pressure at the atmospheric level.

Finally, using a two-phase map, the flow pattern inside Y-jet atomizers was found to be an annular mist flow, a transition between the annular flow and the wispy-annular flow.

Acknowledgments The authors would like to express their appreciation to FAPESP (The State of São Paulo Research Foundation) for its financial support.

References

1. Andreussi P, Tognotti L, de Michele G, Graziadio M (1992) Design and characterization of twin-fluid Y-Jet atomizers. Atomization Sprays 2:45–59
2. Barreras F, Lozano A, Barroso J, Lincheta E (2006) Experimental characterization of industrial twin-fluid atomizers. Atomization Sprays 16:127–145
3. BS 1042 (1989) Measurement of fluid flow in closed conduits, Part 1: Pressure differential devices, Sections 1.1 and 1.2. British Standard Institution, London
4. Collier JG, Thome JR (1996) Convective boiling and condensation, 3th edn. Oxford University, London
5. Ferreira G, García JA, Barreras F, Lozano A, Lincheta E (2009) Design optimization of twin-fluid atomizers with an internal mixing chamber for heavy fuel oils. Fuel Process Technol 90:270–278
6. Ferreira G, Barreras F, Lozano A, García JA, Lincheta E (2009) Effect of the inner two-phase flow on the performance of an industrial twin-fluid nozzle with na internal mixing chamber. Atomization Sprays 19:873–884
7. Graziadio M, Andreussi P, Tognotti L, Zanelli S (1987) Atomization of coal–water fuels by pneumatic internal mixing nozzle. Atomization Spray Technol 3:187–208
8. Griffith P, Wallis GB (1961) Two-phase slug flow. J Heat Transf 83(3):307–320
9. Hewitt GF, Roberts DN (1969) Studies of two-phase flow patterns by simultaneous X-ray and flash photography, AERE-M 2159, HMSO
10. Hewitt GF, Hall-Taylor NS (1970) Annular two-phase flow. Pergamon Press, Oxford
11. JCGM (2008) Guide to the expression of uncertainty in measurement, 2008, Joint Committee for Guides in Metrology. JCGM 100:2008. Evaluation of measurement data
12. Jedelsky J, Jicha M (2008) Unsteadiness in effervescent sprays: a new evaluation method and the influence of operational conditions. Atomization Sprays 18:49–83
13. Lefebvre AH (1980) Airblast atomization. Prog Energy Combust Sci 6:233–261
14. Mullinger PJ, Chigier NA (1974) The design and performance of internal mixing multijet twin fluid atomizers. J Inst Fuel 47:251–261
15. Oshinowo T, Charles ME (1974) Vertical two-phase flow. Can J Chem Eng 52(1):25–35
16. Song SH, Lee SY (1996) Study of atomization mechanism of gas/liquid mixtures flowing through Y-Jet atomizers. Atomization Sprays 6:193–209
17. Song Y, Zhang M (2004) Mathematical modeling and experimental verification of interior gas-liquid flows and outflow atomization process for Y-Jet nozzles. Atomization Sprays 14:437–458
18. Wallis GB (1969) One-dimensional two-phase flow. McGraw-Hill Book Company, New York
19. Zhou Y, Zhang M, Yu J, Zhu X, Peng J (2010) Experimental investigation and model improvement on the atomization performance of single-hole Y-Jet nozzle with high liquid flow rate. Powder Technol 199:248–255